Chapter 6

Data Analysis

Now that a normalized spectrum had finally been obtained, the actual analysis of the data could begin. The principal task here was to determine the parameters of all of the lines in the Ly α forest of HE 0940 and thus produce a suitable sample for studying the proximity effect. As part of that process, an attempt was made to identify as many metal lines as possible so that they could be removed from the Ly α sample.

The present spectrum has complete wavelength coverage of the primary region between the quasar's Ly β and Ly α emission lines at 4158.3 Å and 4928.3 Å, respectively. Lines in the spectrum short of Ly β emission were not fitted unless they belonged to systems containing lines in the primary region of interest. This was because the many, usually stronger Ly α lines and the large amount of blending in the Ly β forest make it difficult to reliably identify all of the higher-order Lyman lines. The resulting contamination in the Ly α sample is difficult to quantify. That is why studies of this type invariably omit the spectral region below 1025.7223 Å in the quasar's rest frame.

Before the labor-intensive process of interactive line fitting could begin, however, two last technical steps were required. The first was to measure the width of the instrumental profile, which is needed as input to the fitting programs. The second was to determine the detection limit for absorption lines in terms of a minimum column density, both for consistency and to avoid wasting time trying to fit noise.

6.1 Instrumental Profile

The observed spectrum is the convolution of the true spectrum with the so-called instrumental profile, so that the observed intensity at a given wavelength λ is

$$I(\lambda) = \int_0^\infty T(\lambda')\, R(\lambda - \lambda')\, d\lambda' \qquad (6.1)$$

where $T(\lambda')$ is the intensity in the true spectrum at λ' and $R(\lambda - \lambda')$ is the response of the spectroscope at a wavelength distance $(\lambda - \lambda')$ from the center (Kitchin 1991).

An estimate of the instrumental profile could be made by measuring the FWHM (full width at half the maximum intensity) of the emission lines in the wavelength-calibration spectra obtained in section 4.8. They spectra were used because an ideal spectroscope and a monochromatic source would produce an infinitely thin emission line at a single wavelength, while diffraction within a real detector causes each emission line to be spread over an entire range of wavelengths. This spread describes the instrumental profile and determines the resolution that can be achieved with the instrument at hand. For a real but optically perfect spectroscope, the instrumental profile would have the shape of the Fourier transform for a regularly spaced finite set of delta functions, modulated by the Fourier transform for a single aperture (Kitchin 1995). Errors in the grating or misalignments in the detector components will obviously lead to devations from this profile and increase the spread even more.

This information is vital for the subsequent measurements of absorption lines because the fitting algorithm must be able to separate out how much of the line width is due to instrumental effects rather than from the instrinsic line width, Doppler broadening and pressure broadening. This can be done on the basis of equation (6.1) if the appropriate input is provided, e.g., the FWHM values at each wavelength.

The FWHM measurements were performed on the three merged WLC frames from which the dispersion coefficients for the three quasar exposures had been obtained. A total of 203 emission lines were chosen in roughly equal intervals along the entire spectrum, and an effort was made to choose only lines that appeared unblended. To avoid selection effects that would lead to differences from one spectrum to another, the exact same transitions were measured in all three spectra.

As often done, the instrumental profile was assumed to be Gaussian, so the line widths were measured by fitting a Gaussian to each emission line using the MIDAS command `CENTER/GAUSS`. The command requires as input the endpoints of the interval in which the fit is to be performed. Strangely enough, it produced different results depending on whether this user input was provided via cursor or via an input table. Measurements of artificially generated Gaussians showed that the former method gave the correct results, so the measurements were done interactively in the graphics window. Fig. 6.1 shows the individual FWHM measurements for one of the three frames. The average FWHM of all the measurements in the three frames, over the wavelength range of the entire spectrum, is 0.26 Å. Using the Doppler relation in equation (5.13) with $\Delta\lambda =$ FWHM and λ_o now the observed (redshifted) wavelength λ_c of the center of each line, these values yielded an average FWHM resolution of 17.7 km s^{-1}.

Fig. 6.1 also shows the linear least-squares fit of the FWHM as a function of the vacuum wavelength in the heliocentric frame. The corresponding estimates for the instrumental resolution as $R = \Delta\lambda/\lambda$ are included merely to show that the linear least-squares fit through the estimated instrumental resolution is, as expected, nearly constant with wavelength. Because of the substantial scatter in the measured FWHM values, the instrumental FWHM assigned to each wavelength in the normalized spectrum was taken as the simple average of the three linear fits at that point.

Some fitting programs (section 6.4) require the line width in terms of the instrumental b value. As with a Gaussian distribution

$$I(\lambda) = I_{\max}\ \exp\left[-\frac{1}{2}\left(\frac{\lambda-\lambda_c}{\sigma}\right)^2\right] \tag{6.2}$$

(where λ_c is the line center), the relation between the full width at half-maximum and standard deviation σ is

$$\sigma = \frac{\frac{1}{2}\,\mathrm{FWHM}}{\sqrt{2\ln 2}} \approx \frac{\mathrm{FWHM}}{2.35482} \tag{6.3}$$

The instrumental b value, which is defined as

$$b = \sigma\sqrt{2} = \frac{\mathrm{FWHM}}{2\sqrt{\ln 2}} \tag{6.4}$$

is most often expressed in units of km s^{-1}. This can be calculated from the FWHM, again with the help of the Doppler relation in equation (5.13), by setting $\Delta\lambda$ equal to b in wavelength units and Δv equal to b in velocity units.

$$b\ [\mathrm{km/s}] \quad = \quad \frac{\sigma\sqrt{2}}{\lambda_c}\,c \quad = \quad \frac{\mathrm{FWHM}\ [\text{Å}]}{2\sqrt{\ln 2}}\ \frac{c\ [\mathrm{km/s}]}{\lambda_c\ [\text{Å}]} \tag{6.5}$$

where λ_c is again the observed central wavelength of the line in question.

The physical meaning of the b value can be envisioned when assuming a Maxwell-Boltzmann velocity distribution (which applies, e.g., to the random thermal motions of atoms of a gas in thermal equilibrium). The resulting line profile is a Gaussian with a full width at half-maximum of

$$\mathrm{FWHM} = 2\sqrt{\ln 2}\ \frac{\lambda_c}{c}\ \sqrt{\frac{2kT}{m}} \tag{6.6}$$

From equation (6.5) we see that

$$b\ [\mathrm{km/s}] = \sqrt{\frac{2kT}{m}}, \tag{6.7}$$

which is also the most probable speed. So, very loosely speaking, b in these units corresponds to the most probable speed in the Maxwell-Boltzmann distribution that would be needed to produce the same line width via Doppler broadening. The difference between the instrumental b value and the b value of a spectral line is that in the former case, the broadening is caused not by particle motions but by the finite spectral resolution of the instrument.

6.2 Astrophysical Quantities

The lines seen in an absorption spectrum can be characterized by the three astrophysical parameters of redshift z, column density N and Doppler width b. Since the main

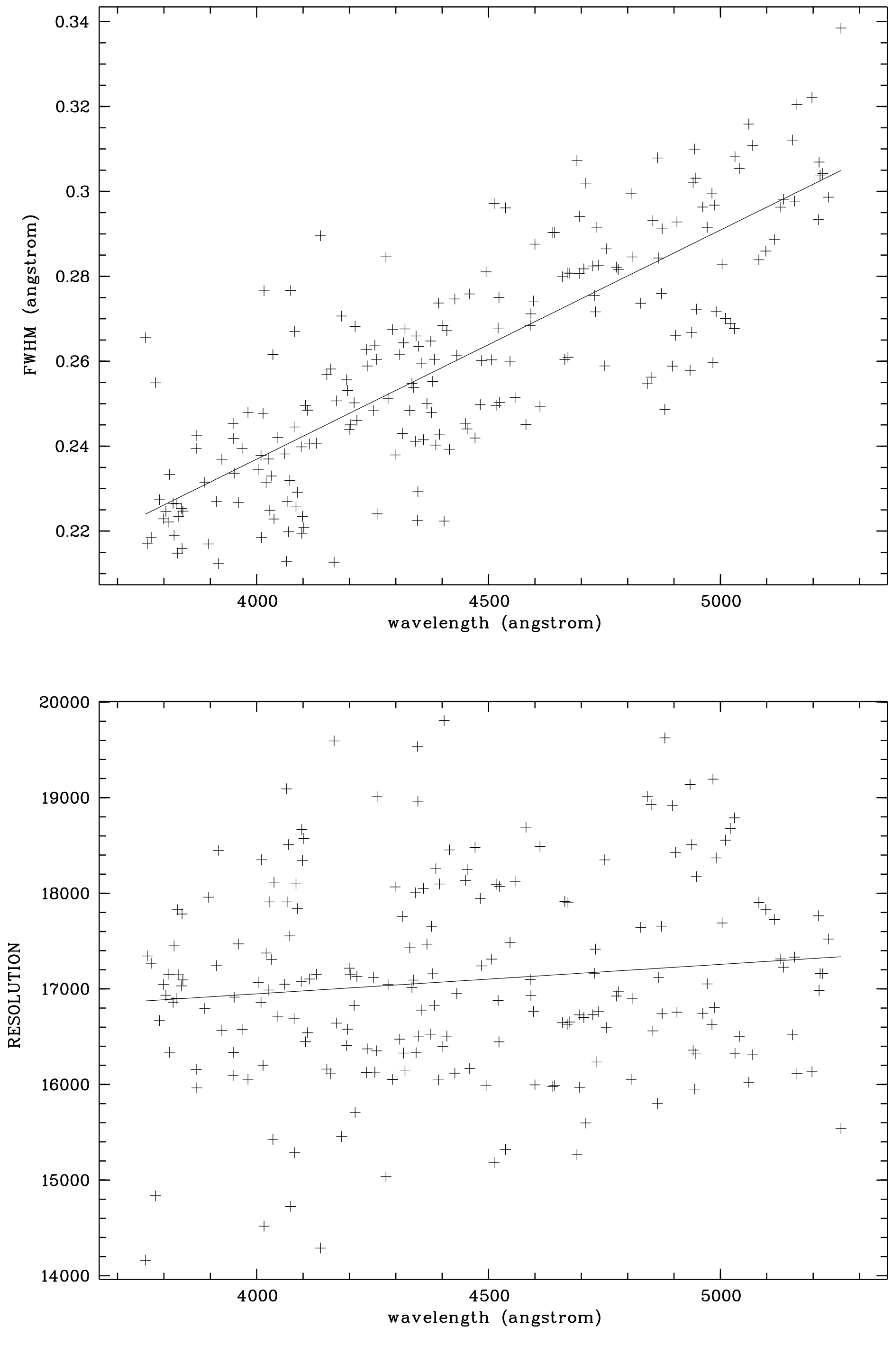

Figure 6.1: *Measurements of instrumental FWHM values for selected arc-lamp emission lines in one of three WLC frames, and corresponding estimates for the instrumental resolution.*

task in the next part of this work was to determine these parameters for the lines in the spectrum of HE 0940, they will be introduced briefly here.

The first absorption-line characteristic to be determined is the wavelength, where we distinguish between the observed wavelength λ and the rest wavelength λ_o in the rest frame where the absorption took place. To facilitate comparison between different spectra, it is often more convenient to use the redshift z, defined by

$$1 + z = \frac{\lambda}{\lambda_o} \tag{6.8}$$

The strength of an absorption line clearly depends on the number of atoms taking part in the absorption. But because the distances between observers and astronomical objects are difficult to determine, it is impractical to use actual densities. Instead, the observable quantity is the column density N, defined by

$$N = \int n_j \, ds \tag{6.9}$$

where n_j is the number density of the absorbing atoms, more precisely the atoms occupying the lower level of the atomic transition $j \to k$. The integral is evaluated over the pathlength ds along the line of sight, so that the column density is equal to the number of absorbing atoms per unit area over the entire distance between the source and the observer.

As already hinted in section 6.1, the b value—which goes by various names, such as Doppler parameter, velocity dispersion or Doppler width—is a measure for the width of a spectral line. However, the b value is not the sole determining factor in the line width. Indeed, the measurements of absorption lines are often complicated by the fact that the column density and the b parameter cannot be determined independently of one another. In order to demonstrate this, some basic concepts of radiative transfer are mentioned below. (Unless otherwise noted, this and the formulas in the rest of section 6.2 were taken from Unsöld and Baschek, 1988).

Optical depth

Given an intial beam of radiation $I_\nu(0)$, defined as the energy passing through the unit area per time interval, frequency and solid angle. As its photons interact with matter along the distance ds, the specific intensity I_ν changes by the amount

$$dI_\nu = -\kappa_\nu I_\nu \, ds + \varepsilon_\nu \, ds \tag{6.10}$$

where κ_ν and ε_ν are the so-called absorption and emission coefficients, respectively. The optical depth is defined by

$$\tau_\nu = \int \kappa_\nu \, ds, \tag{6.11}$$

with $\tau_\nu = 0$ at the observer. Thus the specific intensity reaching an observer through a region of total optical thickness τ_{ν_r} is

$$I_\nu = I_\nu(0)\, e^{-\tau_\nu} + \int_0^{\tau_{\nu_r}} \frac{\varepsilon_\nu}{\kappa_\nu}\, e^{-\tau_\nu} d\tau_\nu \tag{6.12}$$

(Spitzer 1978). In the case of pure absorption, the integral on the right is zero. If we also neglect stimulated emission (because otherwise it would be included as negative absorption), the optical depth can be expressed in terms of atomic constants in SI units as

$$\tau_\nu = \pi r_e c\, N f_{jk}\, \phi(\nu) \tag{6.13}$$

where $r_e = e^2/(4\pi\epsilon_o m_e c^2) = 2.817941$ fm is the classical electron radius, f_{jk} is the upward oscillator strength for the transition $j \to k$, and $\phi(\nu)$ is the line profile function.

Line Profiles

The integral of the line profile function $\phi(\nu)$ over the line is normalized to unity,

$$\int \phi(\nu)\, d\nu = 1, \tag{6.14}$$

while the profile function itself is a complicated function of the distance $(\nu - \nu_c)$ from the center ν_c of the line. It determines the shape of the line and depends on the physical processes taking place in the gas along the line of sight.

The line profile due to natural line broadening, which results from the intrinsic width of energy levels due to their finite lifetimes, is the Lorentz or damping profile

$$L(\nu) = \frac{\gamma}{4\pi^2\,(\nu - \nu_c)^2 + \gamma^2/4} \tag{6.15}$$

where γ is the damping constant and ν_c is the frequency of the line center. Pressure broadening due to nearby atoms also produces this profile in weak absorption lines, in which case γ becomes the sum of the damping constants for each process.

In addition to the natural line broadening and the pressure broadening, there is also the Doppler broadening due to the thermal, possibly turbulent velocities of the absorbing atoms along the line of sight. Assuming these atoms have a Maxwell-Boltzmann velocity distribution, then the profile function assumes a Doppler profile

$$D(\nu) = \frac{c/\nu_c}{b\sqrt{\pi}}\, e^{-\left[\frac{c(\nu-\nu_c)}{b\nu_c}\right]^2} \tag{6.16}$$

For purely thermal motions, $b^2 = {b_k}^2 = 2kT/m$. But Gaussian-distributed turbulent motion with a velocity dispersion b_T can also be accomodated, by using

$$b^2 = {b_k}^2 + {b_T}^2 \tag{6.17}$$

instead.

The combined effects of natural line broadening, pressure broadening and Doppler broadening are described by convolving the two profiles to yield the profile function

$$\phi(\nu) = \int L(\nu - \nu')\, D(\nu')\, d\nu' \tag{6.18}$$

which, with a slightly different normalization, is called the Voigt profile. As mentioned earlier in equation (6.1), the observed spectrum will itself be the convolution of the intrinsic line profile with the instrumental profile.

Near the center of the line, where the Doppler profile is much wider than the damping profile, the Doppler core dominates with the term obtained by expressing equations (6.13) and (6.16) in wavelength units:

$$\tau_\nu = \sqrt{\pi}\, r_e\, N f_{jk}\, \frac{c\lambda_c}{b}\, e^{-\left[\frac{c(\lambda-\lambda_c)}{b\lambda_c}\right]^2} \tag{6.19}$$

If the column densities are small, the lines remain relatively narrow and the area covered by the line increases proportionally to the column density; the line is said to be on the linear part of the so-called curve of growth. But at sufficiently large column densities, the line center becomes optically thick, and the growth in line strength with column density slows considerably. Finally, at even higher column densities, the rate increases a bit because pressure broadening in the saturated line leads to the appearance of the so-called damping wings, where the Lorentz profile dominates. Neglecting the second term in the denominator of equation (6.15), the optical depth in the damping wings is

$$\tau_\nu \approx \frac{r_e}{4\pi}\, N f_{jk}\, \gamma\, \frac{{\lambda_c}^4}{c\,(\lambda - \lambda_c)^2} \tag{6.20}$$

where the approximation $\lambda^2 {\lambda_c}^2 \approx {\lambda_c}^4$ can be made for optical wavelengths.

Equivalent width

One last concept should be mentioned, that of the equivalent width W_λ. It is defined as

$$W_\lambda = \int \left[\frac{I_\lambda(0) - I_\lambda}{I_\lambda(0)}\right] d\lambda = \int \left[1 - e^{-\tau_\lambda}\right] d\lambda \tag{6.21}$$

where the specific intensity I_λ and optical depth τ_λ are now defined in wavelength terms and the integral is evaluated over the entire absorption line. If we visualize a rectangle in a normalized spectrum whose height is equal to 1 and whose width in wavelength units is equal to W_λ, it will have the same area as that covered in the spectrum by the line itself. Lower-resolution spectra, which cannot resolve lines sufficiently to fit the Voigt profile and thus determine N and b, measure W_λ instead. The equivalent width is independent of the instrumental resolution because it represents the fraction of energy removed from the spectrum by an absorption line; so it is a good measure for the line strength, regardless of the resolution. That is why it was used to determine the minimum detection limit in this spectrum (section 6.3).

6.3 Minimum Detection Limit

In order to distinguish small lines from noise, the significance of an absorption line was assessed according to its equivalent width W_λ. A $5\,\sigma$ detection limit was chosen, where the $1\,\sigma$ level was given by

$$\sigma_{\mathrm{W}} = \frac{\mathrm{FWHM}}{\langle\,\mathrm{S/N}\,\rangle} \tag{6.22}$$

(Caulet 1989). The FWHM is the instrumental resolution, and $\langle\,\mathrm{S/N}\,\rangle$ is the mean local signal-to-noise ratio, at the location where a given absorption line is thought to appear.

The FWHM values used were those assigned to each wavelength as described in section 6.1. The mean signal-to-noise ratio was determined by selecting featureless regions at regular intervals wherever possible throughout the spectrum; the standard deviation of the flux values within that region was taken as the local measure of the noise, while the mean signal-to-noise ratio there was simply the inverse standard deviation because the spectrum was already normalized. Finally, the sizes of the selected regions were plotted against the $\langle\,\mathrm{S/N}\,\rangle$ to ensure that there was no correlation between the size of the region chosen and the standard devation, as might have been present had the regions been too small.

This method was chosen rather than the simpler one of merely dividing the flux by the errors in the normalized frames. Because the errors calculated according to error propagation included offset errors such as that for the bias level or background subtraction, they were significantly higher—by a factor of about 1.5 on average—than the actual fluctuations in the spectrum's continuum.

One additional step was necessary to relate this minimum equivalent width to the column densities delivered by the line-fitting programs. If we define an equivalent width W_ν in frequency units,

$$W_\nu \;=\; \int \left[\frac{I_\nu(0) - I_\nu}{I_\nu(0)}\right] d\nu \;=\; \int \left[1 - e^{-\tau_\nu}\right] d\nu \tag{6.23}$$

then it is possible, in principle, to insert equations (6.13) and (6.18) for τ_ν and try to evaluate this integral for W_ν. In practice, however, it was much easier to use an approximation (Spitzer 1978) which takes advantage of the fact that the weak lines being considered here have optical depths $\tau \ll 1$. In this case, the equivalent width in equation (6.21) becomes

$$W_\lambda \;=\; \frac{{\lambda_o}^2}{c} \int \left[1 - e^{-\tau_\nu}\right] d\nu \;\approx\; \frac{{\lambda_o}^2}{c} \int \tau_\nu \, d\nu \tag{6.24}$$

where the middle term in brackets could be expanded and approximated by $e^{-\tau_\nu} \approx 1 - \tau_\nu$ because $\tau_\nu \ll 1$. Along with equations (6.13) and (6.14), this yields

$$W_\lambda \approx \pi r_e \, N f_{jk} \, {\lambda_o}^2 \tag{6.25}$$

Therefore the column density and the equivalent width of optically thin lines are related by

$$N \approx \frac{1}{\pi r_e f_{jk}} \frac{W_\lambda}{\lambda_o^2} = 1.130 \times 10^{20} \text{ Å cm}^{-2} \frac{W_\lambda}{\lambda_o^2 f_{jk}} \tag{6.26}$$

$$N_{\rm HI} \approx 1.838 \times 10^{14} \text{ cm}^{-2} \text{ Å}^{-1} W_\lambda \tag{6.27}$$

where the oscillator strength $f_{jk} = 0.416$ and rest wavelength $\lambda_o = 1215.6701$ Å used in equation (6.27) are specifically for Ly α lines (Verner et al. 1994).

Since equations (6.26) and (6.27) are valid in the rest frame of the absorption line, care must be taken to correct for the effects of cosmological expansion. Just as with the observed wavelength, the observed equivalent width is a factor of $(1 + z)$ larger than the rest-frame equivalent width (Weedman 1986). Thus the only features in the spectrum toward HE 0940 that were identified as Ly α lines were those at the $5\,\sigma$ significance level, which equation (6.27) says are those with column densities

$$N_{\rm HI} \geq \frac{1.838 \times 10^{20} \text{ cm}^{-2} \text{ Å}^{-1}}{1+z} \frac{5 \times \text{FWHM}}{\langle \text{S/N} \rangle} \tag{6.28}$$

The minimum column density for Ly α lines in the spectrum as a whole ranged from log N_{min} = 12.6 at 3800Å to log N_{min} = 12.1 at 5000 Å. In the pure Ly α forest, the detection limit went from log N_{min} = 12.5 at the short-wavelength end down to log N_{min} = 12.2 at the long-wavelength end.

6.4 Line-Fitting Programs

Two fitting programs were used to fit Voigt profiles to the absorption lines in the normalized spectrum of HE 0940. The first was a version of Xvoigt, copyright 1994, written by David Mar at the University of Sydney. Using a text file containing the normalized spectrum as input, Xvoigt asks for the central wavelength (in Å), the size (in km s^{-1}) of the spectral region to be displayed, and the instrumental b value (in km s^{-1}) for that spectral region. It then plots this region on the screen, along with an arbitrary overlayed fit and its current N and b values. These values can be changed by moving the appropriate scroll bars with the mouse. Thus the fit is adjusted interactively until the user obtains what is judged (by eye) to be the best fit. The residuals of the fit can also be plotted to assist the user in making this decision.

Xvoigt allows the fitting of absorption lines by a superposition of more than one Voigt profile. Selecting an on-screen button and typing the central wavelength of the new component makes Xvoigt calculate and display the composite profile. Different atomic transitions of the same ion can also be fit simultaneously and viewed by toggling the check marks in the appropriately labeled boxes.

Although fitting absorption lines manually using Xvoigt provided a good "feel" for how N and b values affect the line profile, the main fitting program used in the analysis was FITLYMAN, a package in the Lyman context of MIDAS whose code was developed at the Osservatorio Astronomico di Roma. Like Xvoigt, FITLYMAN fits Voigt profiles to absorption lines in a normalized spectrum; but rather than relying on user judgments, the fit is obtained through the numerical minimization of χ^2 (Fontana and Ballester 1995).

The line parameters used by FITLYMAN are the observed central wavelength λ_c, the column density N and the Doppler broadening b (which actually consists of two parameters, b_k and b_T; see equation 6.17). The measured flux in the spectrum is written in FITLYMAN as

$$I_\lambda = I_\lambda(0)\, e^{-\tau_\lambda} \tag{6.29}$$

$$\text{with} \quad \tau_\lambda = \sqrt{\pi}\, r_e\, N f_{jk}\, \frac{c\lambda_o}{b\sqrt{2\ln 2}}\, H(a,u) \tag{6.30}$$

where $H(a,u)$ is the equivalent of the line profile in equation (6.18), but expressed here in terms of wavelengths and with a different normalization.

$$H(a,u) = \int_{-\infty}^{\infty} \frac{e^{-y^2}}{a^2 + (u-y)^2}\, dy \tag{6.31}$$

$$a = \frac{\gamma\lambda_c}{4\pi b} \tag{6.32}$$

$$u = \frac{c\,(\lambda_c - \lambda)}{b\lambda_c\sqrt{2\ln 2}} \tag{6.33}$$

The atomic parameters needed (rest wavelength λ_o, oscillator strength f_{jk} and damping constant γ) are taken from the table atompar.tbl in the same directory. The function is fit to the data in such a way as to minimize the chi-square, which is defined for a set of binned data in j histogram bins as

$$\chi^2 \equiv \sum_{i=1}^{j} \frac{[\,h(x_i) - nP(x_i)\,]^2}{\sigma_i(h)^2} = \sum_{i=1}^{j} \frac{[\,h(x_i) - nP(x_i)\,]^2}{nP(x_i)} \tag{6.34}$$

where n is the total number of measurements, $h(x_i)$ is the frequency or observed number of counts in bin i, $P(x_i)$ is the probability of observing the value x_i in a random measurement, $nP(x_i)$ is the expected number of measurements in bin i, and $\sigma_i(h)$ is the standard deviation associated with the uncertainty $h(x_i)$ in the observed counts. Since fluctuations in the observed counts result from the statistical probabilities of taking random samples of a finite number of items, they follow a Poisson distribution with $nP(x_i)$ as mean (Bevington and Robinson 1992). And since the variance in a Poisson distribution is equal to the mean, $\sigma_i(h)^2$ is equal to $nP(x_i)$. Thus the numerator in equation (6.34) is simply the square of the difference between the expected and observed counts in each bin, while the denominator is the number of expected counts.

The actual minimization is performed for FITLYMAN by Minuit, a Fortran 77 package that was developed at the European Laboratory for Particle Physics (CERN). Minuit finds the minimum value of a user-defined multi-parameter function and analyzes the shape of the function around that minimum. The parameters in the function can be kept constant, allowed to vary freely, or allowed to take on any value within certain limits. Parameters that are variable can also be held fixed and later released at any given time during the minimization.

The Minuit version used by FITLYMAN can handle functions with up to 100 parameters, of which not more than 50 can be variable at one time (James 1994). FITLYMAN, in turn, currently allows for the simultaneous fit of up to 50 independent parameters which can be either fixed at a constant value or allowed to vary freely during the entire fitting process. Perhaps the most important feature here is that the user can specify the relations of the four line parameters between any lines in a given fit. For example, lines can be forced to share the same redshift z, so that there is only one independent parameter for their wavelengths. Or, if transitions from the same ion are defined as a multiplet group in FITLYMAN, they will be constrained to have the same z, N and b_k values; with the default b_T of zero for all lines, this results in only four independent parameters for the entire group. Another option is to require a common temperature, which forces the b_k values of the lines to scale with the square root of the ion masses (which are also stored in atompar.tbl). In general, any of the parameters can be either varied freely, assigned to the same variable, or kept fixed at a constant value. The user can simultaneously fit up to 16 lines or more, depending on the number of indendent parameters.

In addition to these user-specified conditions and the initial values for all of the independent variables, FITLYMAN needs to know the Minuit method and the boundaries of the wavelength intervals to be used in the χ^2 calculations. The information is usually entered via the menu-driven interface, but it can also be provided by tables having the same format as the output tables produced by FITLYMAN (these have the suffixes LYPAR.tbl, LYMIN.tbl and LYLIM.tbl).

6.5 Fit Results

Since there was often no continuum between two neighboring absorption lines, the spectrum was divided into 113 fit regions. Each such absorption region contained as many continuum points on each end, and as few absorption lines, as possible.

Every line or group of lines was first fit by hand using Xvoigt. The results were then used as the initial values in FITLYMAN. The output of the χ^2 minimization consisted of the line parameters λ, N and b, the error in each parameter, the reduced χ^2 of the fit, and the probability of χ^2 exceeding that value for the given number of degrees of freedom. If the result was not very good, additional components were added to the fit to improve the χ^2 value. Thus the probability for all of the final fits was greater than 96%. No additional Voigt profiles were added if they increased the χ^2 of the fit. In retrospect, however, this criterion alone was probably not enough to avoid over-fitting (see section 7.2).

In the end, a total of 382 lines were fitted within the Ly α forest between Ly β emission at $\lambda_{obs} = 4158.3$ Åand Ly α emission at $\lambda_{obs} = 4928.3$ Å, as were five Ly α lines just redward of that. Wherever possible, Ly β lines were used to constrain the much less reliable fits of saturated Ly α lines. There were also a number of metal lines present within the forest (see section 6.7), and all of them were fit simultaneously with any other transitions that could be found at the same redshift. The same was done for the two Ly α lines within the forest that had corresponding metal lines. Thus an additional 60 lines outside of the primary region of interest were included in the fits. The synthetic spectrum resulting from the line profiles of all of the fits in the Ly α forest can be seen in Appendix B.

Appendix C lists the line parameters for all of the fits according to wavelength. The errors quoted there were obtained by FITLYMAN using the Minuit command `HESSE`, which calculates them by inverting the covariance matrix. This method was used for convenience: it is the default in FITLYMAN, and the resulting error intervals are symmetric. Although the Minuit command `MINOS` has the advantage of taking both parameter correlations and non-linearities into account, it requires more computing time and yields errors of the form $x^{+\sigma_1}_{-\sigma_2}$.

6.6 Sources of Error

Fontana and Ballester (1995) describe the extensive tests performed on simulated data to assess the stability and accuracy of the results produced by FITLYMAN. The fits achieved high accuracy for unsaturated lines, but as the lines became moderately saturated the fit values showed a larger dispersion as well as the typical anti-correlation between N and b values, so that a line with known parameters might be fit using a larger N and a smaller b or vice versa. Once damping wings began to appear, however, the fits became much more precise. They worsened again considerably after the lines became so strongly saturated that the b value was practically undetermined. Though lower signal-to-noise ratios seemed to increase the possible spread of fitted values in all of these cases, no severe systematic effects could be found.

The problems in fitting saturated lines in particular were confirmed within the present spectrum. Not only were the errors for each of the line parameters much greater, but the χ^2 limit was not always useful in distinguishing between two fits that looked very similar but had very different parameters.

Fontana and Ballester mention two strategies that can improve the accuracy of the fits. The first is to take advantage of the presence of several transitions in a single system wherever possible, because their tests showed that such simultaneous fits significantly increased the precision. That is why, in the spectrum of HE 0940, Ly β lines were used to constrain Ly α fits, and why all of the transitions in the metal systems were invariably fit together as a group.

The second strategy involves the proper choice of the fit interval in which to compute χ^2. The FITLYMAN simulations showed severe systematic effects, particularly for saturated lines, when the limits of the interval were chosen inside the line. The fit intervals in this spectrum were therefore made as wide as possible in all cases, even though the high line density often made it impossible to include many continuum points on the edges of the fits.

The initial fitting with Xvoigt constituted the third strategy that was adopted in an attempt to achieve the best fit results under these conditions. Fontana and Ballester claim that the FITLYMAN algorithm is rather insensitive to the initial values but do admit that in more complex situations involving blends, "it may be necessary to provide reasonable initial values to obtain the correct answer." A few cursory fits of saturated lines in the current spectrum confirmed that different initial values could lead to different, sometimes unphysical, fit results for the same region. The hope was that a reasonable first fit with Xvoigt helped reduce the choice between local χ^2 minima in different regions of parameter space. But is not clear whether such subjective initial guesses really led to better fits.

Even more serious than the errors resulting from uncertainties in the fits themselves is the problem of line blending. As explained by Kirkman and Tytler (1997), line blending occurs when the instrumental resolution is too low to resolve two (or more) lines. They cite the example of several discrete clouds, tens of kiloparsecs apart and each with a small b value. In a spectrum of a certain resolution, these clouds would appear as a single Voigt profile and be taken for a single localized cloud with a high b value. For these reasons, it was often unclear how many components should be used to fit an absorption line in the spectrum of HE 0940. There was a clear trend in which the χ^2 decreased, but the errors in the individual parameters increased, as more components were added to a fit.

Finally, it should be mentioned that the line parameters obtained in the Voigt-profile fitting do not directly describe the actual physical situation of the absorbing gas. The assumptions implicit in the line-blending example cited above, and in the Voigt-profile decomposition in general, are probably not completely valid. As Gardner et al. (1997) have pointed out, recent theoretical work using gas dynamics, radiative cooling and photoionization have undermined the physical picture of discrete Ly α "clouds," each characterized by a single velocity dispersion b. The current theoretical models show absorbing systems that "merge continuously into a smoothly fluctuating background, often contain gas at a range of temperatures, and are usually broadened in frequency space by coherent velocity flows that do not resemble Gaussian turbulence." Nevertheless, these authors add that any spectrum can be described phenomenologically by a superposition of Voigt-profile lines. The key question at that point becomes how the Voigt-profile components and line parameters are related to the actual physical state of the absorbing gas. Theoretically, this can then be deduced by processing simulated spectra in the same way as observed spectra like the one at hand.

6.7 Heavy-Element Systems

Only a few heavy-element systems were expected to be found among the hundreds of lines in the Ly α forest. Nevertheless, an attempt was made to identify as many metal lines as possible in order to reduce the contamination of the Ly α sample.

The standard method for locating heavy-element systems is to search all available wavelengths for significant excesses of identifications at particular redshifts. A simple way to do this would be to apply an automated line-finding and -fitting program to the entire spectrum and then to look for peaks in the histogram of the redshift values. But in this case it was not judged worth the effort to fit the entire spectrum blueward of Ly β emission using the very time-consuming methods described in section 6.4.

So, in the absence of automated line-fitting programs, the search for metal lines was done by means of a simple but effective interactive MIDAS procedure written for this purpose. It displays the desired spectral region in the top half of the graphics window, then asks the user to click on an absorption line with the mouse and enter its assumed identification. When the name of a second transition is entered, the relevant spectral region is plotted in the bottom half of the graphics window along with a vertical line indicating the position at which the desired line would be expected to appear. The originally chosen location is also marked with a vertical line so that the user can judge the positions more closely, optionally select a new location more in the center or more on the wings of the reference line, and see how this would change the position for the expected transition. A mini-menu allows quick navigation between cursor selection, searches for other transitions at the same redshift, and plotting of a new spectral region. No information on relative line strengths was used in the initial search, but this procedure made it possible to check closely the positions of candidate lines and thus rule out most possibilities.

Given a Ly α line with the observed wavelength λ_{obs} in a spectrum covering the wavelength range $[\lambda_{min}, \lambda_{max}]$. The corresponding line of another transition with rest wavelength λ_m will fall within range of the spectrum only if

$$\lambda_{min} \ \leq \ \frac{\lambda_{obs}}{1215.67\ \text{Å}} \ \leq \ \lambda_{max} \tag{6.35}$$

Alternatively, the Ly α of a given metal line will appear in the spectrum only if

$$\frac{\lambda_{min}}{\lambda_m}\, 1215.67\ \text{Å} \ \leq \lambda_{obs} \leq \frac{\lambda_{max}}{\lambda_m}\, 1215.67\ \text{Å} \tag{6.36}$$

Unfortunately, the maximum of the spectral coverage at 5240 Å meant that no Ly α in the entire spectrum could be observed together with its possible Al II, Al III, Fe II or

Mg II lines, which are among the stronger and hence more commonly seen metal lines. None of the Ly α lines in the primary region of the Ly α forest could have C IV lines present in the spectrum either, although C IV lines were within range of the spectral coverage for Ly α lines with $\lambda_{obs} \leq 4142$ Å.

For the purposes of this study, metal systems were identified using the following criteria:

1. If the Ly α was in range of the spectrum, it had to be observed.
2. If the Ly α was not in range, at least one unblended doublet had to be present.
3. In either case, a simultaneous FITLYMAN fit of all transitions in the system had to yield a reasonable fit, defined as one with probability $P > 96\%$ and not too many improbable blends.

Although multiple lines of the same ion were constrained to share the same redshift, column density and b value, no other conditions were set on the metallicities or ratios of ionization species.

The general strategy in the search for metal lines was to begin with the isolated lines redward of Ly α emission, in this case the two obvious groups of C IV doublets at ~5160 Å and ~4990 Å and the small Si IV doublet at 5112, 5145 Å. Using the list of strong lines expected in quasar absorption systems by Verner et al. (1994), further members of these systems were sought using the interactive MIDAS procedure described above.

The next step was to examine all of the strongest saturated lines, both inside and outside of the Ly α forest, on the assumption that these were the most likely to show corresponding metal lines. First the C IV $\lambda\lambda 1548, 1550$ doublet was sought, if it was in range; then the Si IV $\lambda\lambda 1393, 1402$ doublet and the Si III $\lambda 1206$ and C II $\lambda 1334$ lines. These were the only metal ions found in the end, although others such as Si II and N V were also checked.

A total of five heavy-element systems were identified in this way. An additional C IV system was noticed at $z \approx 2.83$ because of the large complex of strongly saturated lines between 4644 Å and 4664 Å. The corresponding C IV absorption can be seen from about 5920 Å to about 5950 Å in the 1.52-meter spectrum of HE 0940 (Fig. 2.1). Since this feature is not resolved, however, no further information could be obtained on this system.[1]

Other extensive but more random searches for metal systems produced no additional identifications according to the criteria listed above. The absorption lines that could be identified as belonging to possible metal systems on the basis of this spectrum alone are summarized in Table 6.1.

[1] Since then, a higher-resolution spectrum than the one in Figure 2.1 has been obtained at the ESO 1.52-meter telescope. It extends up to 7500 Åand shows more details of the complex C IV system at $z \sim 2.82$. Additional metal systems have thus been identified: there is a strong, probably damped Ly α system at $z = 1.9185$ with Fe II, Si II, Al III and other metal lines, as well an Mg II system at $z = 1.06$ (D. Reimers, private communication).

ID	z	λ_{obs} (Å)	σ_λ	log N (cm^{-2})	σ_N	b (km s^{-1})	σ_b
H I 1215	2.174456	3859.09	0.02	18.30	0.06	29.7	1.0
C II 1334	2.174456	4236.41	0.02	13.21	0.11	7.9	5.7
Si IV 1393	2.174456	4424.41	0.02	13.34	0.04	22.8	3.0
Si IV 1402	2.174456	4453.03	0.02	13.34	0.04	22.8	3.0
C IV 1548	2.174587	4914.88	0.01	14.25	0.02	23.6	0.9
C IV 1550	2.174587	4923.06	0.01	14.25	0.02	23.6	0.9
H I 1215	2.220397	3914.94	0.05	14.38	0.14	54.6	7.1
C IV 1548	2.220396	4985.80	0.06	13.44	0.05	41.6	5.1
C IV 1550	2.220397	4994.09	0.06	13.44	0.05	41.6	5.1
Si III 1206	2.220513	3885.55	0.01	12.64	0.12	29.2	12.0
H I 1215	2.220513	3915.08	0.01	16.13	5.51	17.3	17.6
Si IV 1393	2.220513	4488.61	0.01	12.55	0.10	9.3	6.3
Si IV 1402	2.220513	4517.64	0.01	12.55	0.10	9.3	6.3
C IV 1548	2.220513	4985.98	0.01	13.74	0.03	8.9	1.0
C IV 1550	2.220513	4994.28	0.01	13.74	0.03	8.9	1.0
Si III 1206	2.221298	3886.50	0.02	13.13	0.15	27.9	5.0
H I 1215	2.221298	3916.04	0.02	13.86	0.34	54.2	19.3
Si IV 1393	2.221298	4489.70	0.02	12.99	0.06	29.8	5.6
Si IV 1402	2.221298	4518.74	0.02	12.99	0.06	29.8	5.6
C IV 1548	2.221298	4987.20	0.02	13.57	0.04	14.8	2.9
C IV 1550	2.221298	4995.49	0.02	13.57	0.04	14.8	2.9
Si III 1206	2.221561	3886.81	0.02	12.67	0.58	38.2	25.4
H I 1215	2.221561	3916.36	0.02	13.88	0.22	21.9	10.1
C IV 1548	2.221561	4987.60	0.02	13.21	0.13	5.5	1.3
C IV 1550	2.221561	4995.90	0.02	13.21	0.13	5.5	1.3

Table 6.1: *Heavy-element systems in the spectrum toward HE 0940–1050.*

ID	z	λ_{obs} (Å)	σ_λ	log N (cm^{-2})	σ_N	b (km s^{-1})	σ_b
Si IV 1393	2.329162	4640.04	0.01	13.71	0.04	23.3	1.4
Si IV 1402	2.329162	4670.05	0.01	13.71	0.04	23.3	1.4
C IV 1548	2.329162	5154.19	0.01	14.75	0.13	19.3	1.5
C IV 1550	2.329162	5162.76	0.01	14.75	0.13	19.3	1.5
Si IV 1393	2.330278	4641.59	0.12	13.17	0.16	25.4	5.6
Si IV 1402	2.330278	4671.61	0.12	13.17	0.16	25.4	5.6
C IV 1548	2.330278	5155.92	0.13	14.19	0.12	35.9	5.0
C IV 1550	2.330279	5164.50	0.13	14.19	0.12	35.9	5.0
Si IV 1393	2.330575	4642.01	0.03	13.36	0.11	14.3	3.2
Si IV 1402	2.330575	4672.03	0.03	13.36	0.11	14.3	3.2
C IV 1548	2.330575	5156.38	0.04	14.03	0.16	13.7	4.3
C IV 1550	2.330575	5164.96	0.04	14.03	0.16	13.7	4.3
Si IV 1393	2.331016	4642.62	0.06	12.50	0.15	12.8	6.6
Si IV 1402	2.331016	4672.65	0.06	12.50	0.15	12.8	6.6
C IV 1548	2.331016	5157.06	0.07	13.93	0.07	30.3	3.9
C IV 1550	2.331016	5165.64	0.07	13.93	0.07	30.3	3.9
H I 1025	2.667540	3761.88	0.04	15.21	0.12	63.1	5.0
H I 1215	2.667541	4458.52	0.04	15.21	0.12	63.1	5.0
Si III 1206	2.667541	4424.89	0.05	12.94	0.05	24.5	3.3
Si IV 1393	2.667541	5111.65	0.05	12.80	0.06	21.9	4.3
Si IV 1402	2.667541	5144.72	0.05	12.80	0.06	21.9	4.3
H I 1025	2.916881	4017.63	0.01	16.23	0.18	48.9	2.3
H I 1215	2.916881	4761.64	0.01	16.25	0.18	48.9	2.3
Si III 1206	2.916881	4725.72	0.01	13.07	0.06	14.3	1.5

Table 6.1: *Heavy-element systems in the spectrum toward HE 0940–1050, cont.*